Quasi-Elliptic Dual-Band Planar BPF With High-Selectivity and High Inter-Band Isolation for 5G Communications Systems

Muhammad Riaz, Bal S. Virdee, Pancham Shukla, Karim Ouazzane, Muhittin Onadim, and Shahram Salekzamankhani

***Abstract*— A novel dual-band planar bandpass filter structure is presented that exhibits the following characteristics: (i) a quasi-elliptic function response with high passband selectivity; (ii) high inter-band isolation; and (iii) a wide out-of-band rejection. The filter is suitable for highly demanding wireless communications systems where the channel capacity is at a premium. The via-free dual-band filter consists of open-loop resonators that are shunt loaded with a half-wavelength open-circuit stub. The resonators are coupled electromagnetically to the stepped impedance resonators, which are inter-digitally coupled to the input/output feed lines. Altering the dimensions of the two stubs allow modification of the resonant mode and transmission zero frequencies. Measured results validate the filter's performance. The center frequencies of the two passband responses at 4.6 GHz and 5.4 GHz have 3-dB fractional bandwidth of 13.5% and 11.5%, respectively. Insertion-loss at the two passband center frequencies are 1.02 and 0.8 dB, and the return-loss is better than 20 dB. Skirt steepness of the filter is >290 dB/GHz, and isolation between the two closely positioned adjacent bands is better than 35 dB.**

***Index Terms*— Stepped impedance resonator, dual-band filter, quasi-elliptic filter, wideband.**

I. Introduction

WIDEBAND transmission is essential for the next generation of cellular communication systems such as 5G in order to achieve high capacity and high-speed data transmission. An effective technique to achieve this requirement is by using carrier-aggregation (CA) in which multiple discrete frequency bands are combined prior to transmission [1]. In this context, integration of low insertion-loss filters, centered on moderately spaced frequencies, is crucial to achieve CA without increasing the fabrication complexity (and costs) of next-generation mobile handsets. This requirement has created a demand for dual-band microwave bandpass filters (BPF) that possess characteristics of sharp skirt and low insertion-loss for the efficient and flexible utilization of the limited and expensive frequency spectrum [2]. Moreover, dual-band filter with wide stopband is essential for interference management, especially in the scenarios of heterogeneous wireless systems coexistence [3-7].

Use of a high-temperature superconductor (HTS) is one of the effective ways to realize a dual-band filter with these desirable characteristics, however this technology is highly expensive, and the filter size is prohibitively large for portable applications. The simplest way to construct a dual-band bandpass filter (BPF) involves combining two single-band filters. Additional impedance-matching networks may be required. The resulting filter is likely to be undesirably large, and its characteristics (slow roll-off skirts) far from acceptable for practical purposes. Hence, considerable interest has been raised in the development of dual-band filters. Various design approaches investigated have been reported lately, e.g. in [4] a double slot loaded resonator is used to realize a dual bandpass filter with two closely spaced passbands. The length between the two slots and open circuited stubs control the bandwidth of the two passbands. However, miniaturization and simpler filter configuration is achieved here at the expense of poor passband selectivity. Multimode behaviour of stepped impedance resonators (SIR) have previously been exploited in the development of multi-band filters by using open/short-circuited stubs. Other examples of dual-band filter designs implemented using SIRs are reported [5]. Roll-off skirts, frequency selectivity and stopband performance of the above dual and multiband filters are poor for the effective utilization of the frequency spectrum. In addition, the filters are non-contiguous.

This letter presents a novel filter structure implemented with SIR that is loaded with L-shaped shunt open-circuit stubs. The structure generates three transmission zeros that results in a very wide stopband. The L-shaped shunt open-circuit stubs enable control of the three transmission zeros. The structure of the planar bandpass filter (BPF) is simple, via-free and compact. The filter possesses desirable characteristics, i.e.: (i) excellent quasi-elliptical response with a sharp roll-off (>290 dB/GHz); (ii) contiguous response; (iii) low passband insertion-loss; (iv) excellent inter-band isolation; and (v) relatively wide stopband. These characteristics are normally found in cavity and HTS filters.

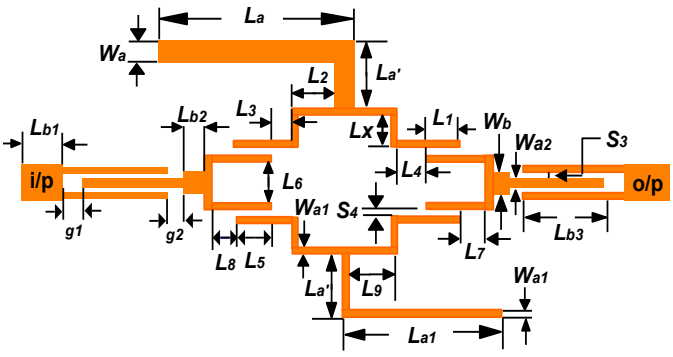

Fig. 1. Microstrip layout structure of the proposed dual wideband bandpass filter where the RF signal is fed from the left-hand side port and extracted from the right-hand side port.

The authors are with Center of Communications Technology in the School of Computing & Digital Media at London Metropolitan University, London, UK. (e-mail: b.virdee@londonmet.ac.uk).

II. Analysis of Stub Loaded Resonator

Configuration of the dual-band BPF, shown in Fig. 1, can be considered essentially consisting of a pair of resonators that are shunt loaded with a half-wavelength open-circuited stub. These resonators are coupled electromagnetically to SIR structures, where the SIRs are inter-digitally coupled to the input/output feedline. Characteristic impedance and electrical length of the resonator and the L-shaped shunt open-circuit stubs, shown in Fig. 2, have different impedances and electrical lengths. The first transmission line has an impedance of Z_1 and an electrical length of θ_1. The vertically loaded stub has an impedance of Z_3 and an electrical length of θ_3. The horizontal open-ended stub has an impedance of Z_2 and an electrical length of θ_2. Open-circuit stubs can be bend by 90° to reduce the lateral size of the structure, as shown in Fig. 1.

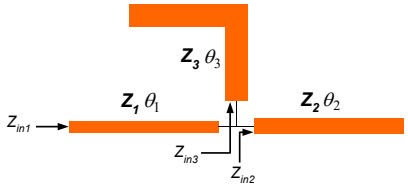

Fig. 2. Microstrip structure of the stub-loaded resonator

Using impedance transformation, the input impedances looking into the horizontal stub and the vertically loaded stub, as labeled in Fig. 2, are:

$$Z_{in2} = -jZ_2 cot\theta_2 \quad \text{and} \quad Z_{in3} = -jZ_3 cot\theta_3 \qquad (1)$$

By combining these equations in parallel, we obtain:

$$Z_L = \frac{-jZ_2C_2Z_3C_3}{(Z_2C_2+Z_3C_3)} \qquad (2)$$

Where $C_2 = cot\theta_2$ and $C_3 = cot\theta_3$. Then application of impedance transformation, the input impedance of the overall resonator is:

$$Z_{in1} = \frac{-jZ_1Z_2C_2Z_3C_3 - jZ_1^2t_1Z_2C_2 - jZ_1^2t_1Z_3C_3}{Z_1Z_2C_2 - Z_1Z_3C_3 - Z_2C_2Z_3C_3t_1} \qquad (3)$$

$Z_{in1} = \infty$ (resonant condition) occurs when:

$$Z_1Z_2C_2 + Z_1Z_3C_3 + Z_2Z_3C_2C_3t_1 = 0 \qquad (4)$$

Where $t_i = tan\theta_i$ and $C_i = cot\theta_i$, $i = 1, 2, 3\ldots$

$$tan(n\theta_2) + tan(n\theta_3) + ktan(n\theta_1) = 0 \qquad (5)$$

Where n is the ratio of resonance frequency f_r to the fundamental resonance f_1; and impedance ratio $k = Z/Z_1$. A preset stub length of θ_1 and θ_2 requires determination of θ_3 to realize the fundamental resonance condition, which can be obtained by solving (5) by putting n = 1. Assuming $Z_2 = Z_3 = Z$ and $\theta_2 = \theta_3 = \theta$ (5) simplifies to:

$$tan(n\theta) + \frac{k}{2}tan(n\theta_1) = 0 \qquad (6)$$

Resonance frequency ratio of higher order modes relative to the fundamental mode of the stub-loaded structure is plotted in Fig. 3(a) as a function of θ_1 and k for a stub length of 120°. The plot reveals the position of the modes are controllable by changing θ_1 and k. Fig. 3(b) shows how the stub length (in degrees) affects the frequency ratio for a fixed value of k. The plot indicates dual-band filter functionality is realizable by employing stub-loaded structure.

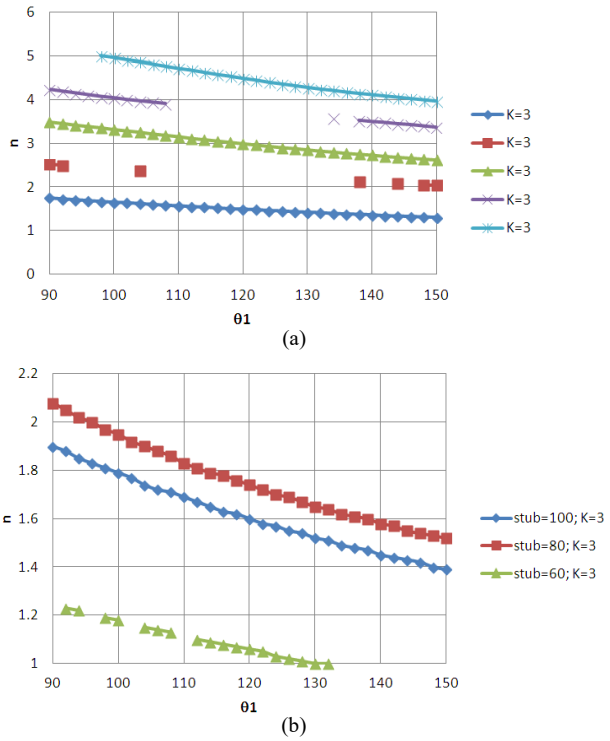

Fig. 3. (a) Solution of resonance frequency ratio of higher order modes relative to the fundamental frequency as a function of θ_1 and k for a stub length of 120°, and (b) Resonance frequency ratio as a function of θ_1 for different stub lengths.

III. Parametric Study and Proposed Filter Design

To gain further insight on the filter configuration it was necessary to conduct a parametric study using Keysight Technologies' ADS™ EM tool. Fig. 4(a) shows that the transmission zeros (f_{Z1} and f_{Z2}) and resonant frequency (f_{even2}) can be controlled by stub length L_a. Resonant frequency f_{odd2} and transmission zero f_{Z3} move towards higher frequency as the stub length L_{a1} is reduced from 8.24 mm to 7.04 mm, as shown in Fig. 4(b). Stub length L_{a1} has negligible effect on f_{odd1} and f_{Z2}. Length L_9 controls f_{even1}, as shown in Fig. 5(a), with negligible effect on f_{odd2}, f_{Z1} and f_{Z2}. Width W_a essentially control the locations of transmission zeros f_{Z1} and f_{Z2} as shown in Fig. 5(b).

The parametric study conducted revealed that the length (L_{b2}) and width (W_b) can adversely affect the out-of-band rejection level of the filter, as shown in Fig. 6. The effect of the interdigital coupled feed length (L_{b3}) on the filter's characteristics in Fig. 7(a) shows the out-of-band rejection level on either side of passband worsen significantly with decrease in L_{b3}. The effect of resonator length (L_1) on filter's performance is shown in Fig. 7(b). When L_1 is reduced from 5.44 mm to 4.54 mm the resonant frequency f_{even1} shifts from 4.46 GHz to 4.62 GHz and f_{odd1} from 4.80 GHz to 5 GHz. Transmission zeros f_{tz1} and f_{tz2} shift upward in frequency by 7% and 2%, respectively, and f_{odd2} by 2%. The upper out-of-band rejection performance of second passband correspondingly deteriorated rapidly from 15 dB to 5 dB. It is

evident from Fig. 8(a) the resonant modes f_{odd1}, f_{even2} and transmission zero f_{tz2} are mainly controlled by resonator length (L_7). Resonant modes f_{odd1}, f_{even2} and transmission zero f_{tz2} move downward in frequency when L_7 is changed from 3.17 mm to 4.37 mm. The consequence of this was a corresponding deterioration of the upper and lower rejection levels from 34 dB to 28 dB. Fig. 8(b) shows the effect of feedline coupling gap (S_3) on the out-of-band rejection. As the coupling gap is increased the out-of-band rejection improves however this is at the expense of steady increase in the passband ripple. The dimensions of the above parameters were carefully optimized so that the filter's overall performance was not compromised.

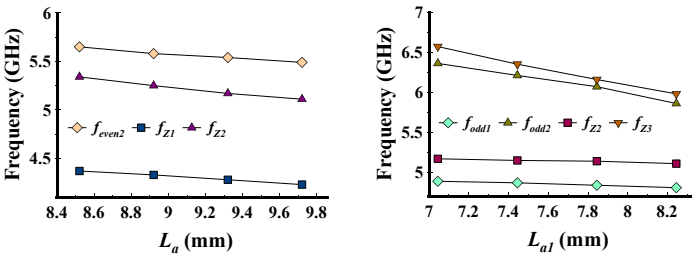

Fig. 4 (a) Effect on the filter's first and second transmission zeros, and second even resonant frequency as a function of open stub length L_a, and (b) Effect on the filter's transmission zeros, even and odd resonant frequencies as a function of open stub length L_{a1}.

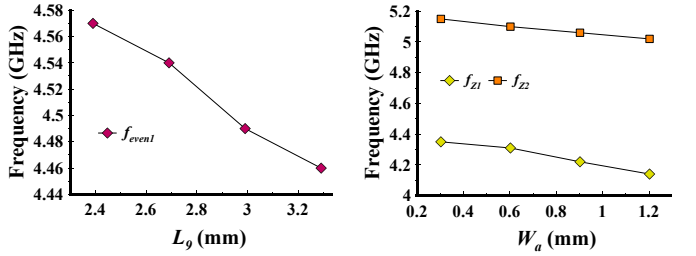

Fig. 5. (a) Even resonant frequency of the filter as a function of resonator length L_9, and (b) Effect on the filter's transmission zeros as a function of width W_a.

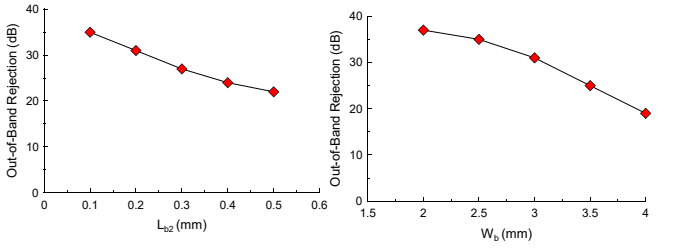

Fig. 6. (a) Out-of-band rejection as a function of length L_{b2}, and (b) Out-of-band rejection as a function of width W_b.

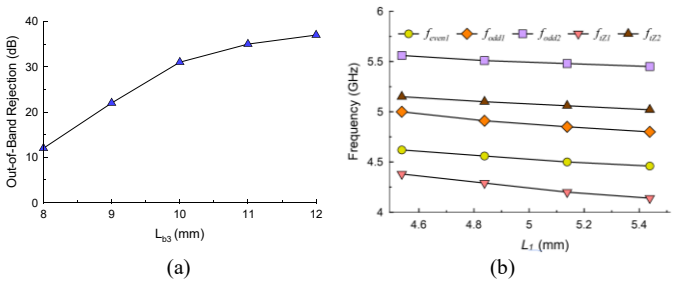

Fig. 7. (a) Out-of-band rejection as a function of interdigital coupled feed length L_{b3}, and (b) Effect on the filter transmission zeros and even and odd resonant frequencies as a function of resonator length (L_1)

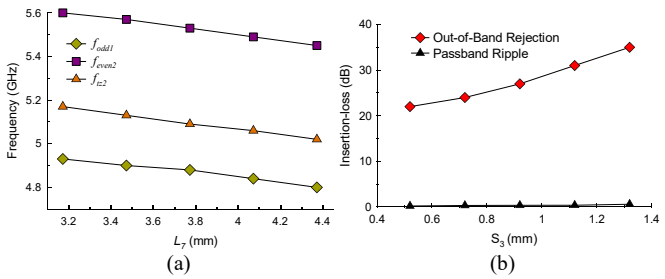

Fig. 8. (a) Effect on the filter transmission zeros and even and odd resonant frequencies as a function of resonator length (L_7), and (b) Frequency response of the proposed filter as a function of feedline coupling gap (S_3).

The design of the proposed filter was determined from the information gained in the above parametric study. The filter can be designed at a normalized notch frequency that splits the two adjacent passbands using the dimensions (in wavelength) given in Table I of the dual-band filter structure shown in Fig. 1.

TABLE I
NORMALIZED DIMENSIONS OF THE DUAL BAND BPF

Parameters	Dimension (λ_o)	Parameters	Dimension (λ_o)
W_a	0.020	g_2	0.003
W_{a1}	0.003	L_1	0.089
W_{a2}	0.014	L_2	0.055
W_b	0.040	L_3	0.029
W_d	0.027	L_4	0.028
L_a	0.172	L_5	0.091
L_a'	0.022	L_6	0.015
L_{a1}	0.137	L_7	0.073
L_{b1}	0.050	L_8	0.069
L_{b2}	0.003	L_9	0.055
L_{b3}	0.167	S_3	0.006
g_1	0.003	S_4	0.004

The BPF in Fig. 1 was designed at arbitrarily dual-band notch frequency of 5 GHz using the normalized dimensions given in Table I. The filter was constructed on Arlon CuClad217LX with thickness of 0.794 mm, ε_r of 2.17 mm, conductor thickness of 35 μm, and loss-tangent of 0.0009. Parametric study enabled optimisation of the filter's performance. The optimised filter parameters (in millimeters) are: W_a = 1.2, W_{a1} = 0.2, W_{a2} = 0.87, W_b = 2.42, W_d = 1.66, L_a

= 10.36, $g_1 = g_2 = 0.2$, $L_a' = 1.314$, $L_{a1} = 8.24$, $L_{b1} = 3$, $L_{b2} = 0.2$, $L_{b3} = 10$, $L_1 = 5.36$, $L_2 = 3.3$, $L_3 = 1.76$, $L_4 = 1.71$, $L_5 = 5.44$, $L_6 = 0.89$, $L_7 = 4.37$, $L_8 = 4.17$, $L_9 = 3.29$, $S_3 = 0.39$, and $S_4 = 0.24$. The fabricated dual-band filter and its measured performance are shown in Figs. 9 & 10, respectively. Center frequency of the two passbands are 4.66 GHz and 5.5 GHz, and their corresponding 3-dB fractional bandwidths are 13% and 12%, respectively. Insertion-loss at the center frequencies are 1.02 and 0.8 dB, whereas the return-loss are better than 20 dB. The three transmission zeros are located at 4.2 GHz, 5.0 GHz and 5.9 GHz respectively, which resulted in a dual-band BPF with sharp selectivity. Table II shows the comparison of the proposed dual-band filter with recently published work. Compared to other filters cited the proposed filter exhibits excellent quasi-elliptic response with sharp roll-off, a contiguous response, excellent inter-band isolation, and a wide stopband.

TABLE II
PERFORMANCE COMPARISON WITH RECENTLY PUBLISHED DUAL BAND BPFS

Ref.	Upper Stopband (GHz)	f_1 / f_2 (GHz)	IL (dB)	FBW (%)	*Roll-off* (dB / GHz)
[8]	4.1–4.7	2.10 / 2.60	0.8 / 1.2	17 / 8.4	26
[9]	2.6–2.9	0.89 / 2.42	0.9 / 1.65	12 / 4.1	66
[10]	3.0–4.8	1.57 / 2.45	1.26 / 2.5	9 / 8.5	65
[11]	3.1–3.4	1.57 / 2.47	0.53 / 0.7	15.3 / 12.7	16
[12]	6.8–8.9	2.40 / 5.80	1.6 / 1.97	4.6 / 3.6	30
[13]	6.1–7.0	2.50 / 5.60	1.3 / 1.97	7 /4.2	30
This work	5.7–8.8	4.60 / 5.40	1.02 / 0.8	13.5 / 11.5	295

Upper Stopband is defined for $S_{21} \geq 20$ dB; f_1 / f_2 = center frequency of dual-band passbands; IL= insertion-loss; and 3-dB FBW = fractional bandwidth.

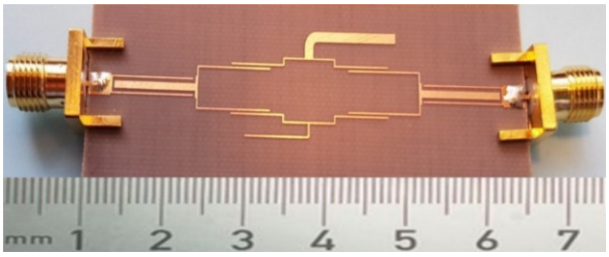

Fig. 9. Photograph of the dual-mode wideband BPF fabricated on CuClad217LX dielectric substrate.

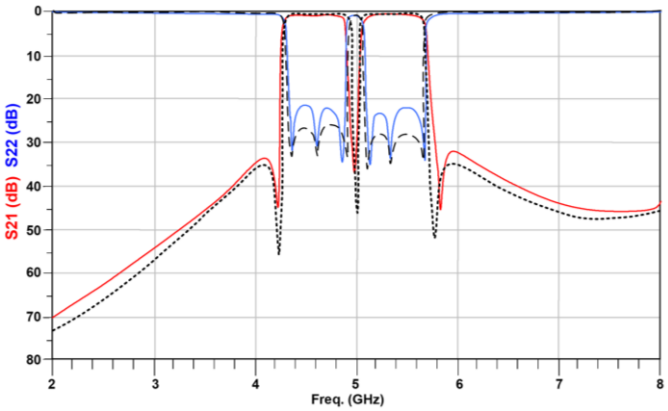

Fig. 10. Measured insertion-loss & return-loss response of the proposed dual-mode BPF. (Dot and dash lines are simulation results.)

IV. CONCLUSION

A novel dual-band bandpass filter based on coupled lines multimode resonator has been demonstrated to exhibit excellent roll-off (>290 dB/GHz), high-selectivity and high inter-band isolation, which is normally found in cavity or HTS filters. The filter configuration generates pentamode, where three modes contribute towards generating the first passband, and the remaining two modes in creating the second passband. The resonant modes and transmission zeros can be tuned precisely by simply modifying the length of the two shunt stubs. The filter exhibits characteristics that make it suitable for RF wireless communication systems with stringent specifications.

REFERENCES

[1] G. Yuan, X. Zhang, W. Wang, Y. Yang, "Carrier aggregation for LTE-advanced mobile communication systems," *IEEE communications Mag.*, 48, 88–93, 2010.

[2] X. Lu, B. Wei, B. Cao, X. Guo, X. Zhang, Z. Song, Y. Heng, Z. Xu, "Design of a high-order dual-band superconducting filter with controllable frequencies and bandwidths," *IEEE Trans. Appl. Supercond.*, 19, 1500205, 2014.

[3] P. Kryszkiewicz, A. Kliks, H. Bogucka, "Small-scale spectrum aggregation and sharing," *IEEE Journal on Selected Areas in Communications*, 34, 2630-2641, 2016.

[4] S. Khani et al. "Compact ultra-wide upper stopband microstrip dual-band BPF using tapered and octagonal loop resonators," *Frequenz*, 2019.

[5] L. Wangshuxing et al., "Dual-band bandpass filter using loop resonator with independently-tunable passband," *Electronics Letters*, 53(25), 1655-1657, 2017.

[6] S. Khani et al., "Tunable compact microstrip dual-band bandpass filter with tapered resonators," *Microwave and Optical Technology Letters*, 60(5), 1256-1261, 2018

[7] S. Khani et al., "Miniaturized microstrip dual-band bandpass filter with wide upper stop-band bandwidth," *Analog Integrated Circuits and Signal Processing*, 98(2), 367-376, 2019.

[8] D. Chen, L. Zhu, C. Cheng, "A novel dual band bandpass filter with closely spaced passbands," *IEEE Microwave and Wireless Components Letters*, 24(1), 38–40, 2014.

[9] S. B. Zhang, L. Zhu, "Synthesis design of dual-band bandpass filters with stepped-impedance resonators," *IEEE Trans. Microw. Theory Tech.*, 61(5), 1812–1819, 2013.

[10] Y. Peng, L. Zhang, J. Fu, Y. Wang, Y. Leng, "Compact dual-band bandpass filter using coupled lines multimode resonators," *IEEE Microwave and Wireless Components Letters*, 25(4), 235–237, 2015.

[11] F. Wei, P.-Y. Qin, J. Guo, "Compact Balance dual and tri-band BPFs based on coupled complementary split-ring resonators (C-CSRR)," *IEEE Microwave and Wireless Components Letters*, 26(2), 107–109, 2016.

[12] Z.-C. Zhang, Q.-X. Chu, F.-C. Chen, "Compact dual-band bandpass filters using open/short-circuited stub-loaded λ/4 resonators," *IEEE Microwave and Wireless Components Letters*, 25(10), 657–689, 2015.

[13] F. Bagci, A. Fernández-Prieto, A. Lujambio, J. Martel, J. Bernal, "Compact balanced dual-band bandpass filter based on modified coupled-embedded resonators," *IEEE Microwave and Wireless Components Letters*, 27(1), 31–33, 2017.